Chinese Chemical Letters 37 (2026) 111016

Contents lists available at ScienceDirect

Chinese Chemical Letters

journal homepage: www.elsevier.com/locate/cclet

Mo, B-induced local structure and electron redistribution of RuO_2 for efficient acidic oxygen evolution

Ziang Shang[a,1], Heyu Sui[b,1], Zeyi Huang[a,1], Xueting Feng[a], Guanzhen Chen[a], Jiena Weng[a], Yu Xiong[c], Yaqiong Su[b,*], Yunhu Han[a,*]

[a] Institute of Flexible Electronics (IFE) and Frontiers Science Center for Flexible Electronics, Northwestern Polytechnical University, Xi'an 710129, China
[b] School of Chemistry, Engineering Research Center of Energy Storage Materials and Devices of Ministry of Education, National Innovation Platform (Center) for Industry-Education Integration of Energy Storage Technology, Xi'an Jiaotong University, Xi'an 710049, China
[c] Chemistry and Chemical Engineering, Central South University, Changsha 410083, China

ARTICLE INFO

Article history:
Received 18 December 2024
Revised 19 February 2025
Accepted 27 February 2025
Available online 27 February 2025

Keywords:
RuO_2
Electrocatalysis
Oxygen evolution reaction
Electronic structure
Proton exchange membrane water electrolyzers

ABSTRACT

Oxygen evolution reaction (OER) is a key reaction in proton exchange membrane water electrolyzers (PEMWEs). Therefore, developing cost-effective acid-stable electrocatalysts to drive efficient OER is crucial. Here, we constructed a RuO_2 electrocatalyst (MoB-RuO_2) co-doped Mo and B atoms, which exhibits excellent OER performance in acidic media. In 0.5 mol/L H_2SO_4, MoB-RuO_2 exhibited a very low overpotential (166 mV) and could be operated stably for more than 550 h at 10 mA/cm^2 current density without significant loss of activity. More than 240 h of stable operation at 200 mA/cm^2 current density was achieved when using MoB-RuO_2 as a PEMWE anode. Experimental and theoretical results demonstrated that the excellent OER activity and stability of MoB-RuO_2 mainly originated from the incorporation of B atoms leading to the coordination unsaturation of the active centre Ru, and the simultaneous doping of Mo and B atoms modulated the electronic structure of Ru, which lowered the covalency of the Ru-O bond, thus making the catalyst exhibit excellent stability.

© 2026 Published by Elsevier B.V. on behalf of Chinese Chemical Society and Institute of Materia Medica, Chinese Academy of Medical Sciences.

As one of the core technologies for energy conversion and storage such as proton exchange membrane water electrolyzers (PEMWEs) [1–3], the oxygen evolution reaction (OER) requires catalysts with extremely high catalytic activity due to the complex multiple proton/electron-coupled steps involved in the process, which results in very slow kinetics of OER [4,5]. In recent years, researchers have made significant progress in developing OER catalysts with high activity in acidic conditions [6,7]. However, due to the harsh operating environment of PEMWEs, catalyst stability is crucial [8,9], and the catalysts that can meet this requirement are almost all catalysts mainly composed of precious metal Ir, which leads to the cost problem that is becoming more and more prominent [10]. Therefore, the development of low-cost, highly active, and stable OER catalysts is imperative for advancing energy conversion and storage technologies. However, significant challenges remain, particularly with regard to OER catalysts that can be stabilised under the practical operating conditions of PEMWEs [11].

The Ru-based catalysts have superior OER activity compared to most reported OER catalysts, and due to the relatively high storage capacity of Ru, the cost is only one-tenth of that of the Ir-based acidic OER catalysts commercially available at present, making them cost-effective catalytic materials for the anode of energy conversion and storage devices, especially for operation under acidic environments [12–14]. Considering this, the development of Ru-based OER catalysts has been favoured by more and more researchers in recent years, especially RuO_2-based acidic OER catalysts, whose activity even exceeds that of most of the Ir-based catalysts, and has been regarded as an ideal alternative to Ir-based catalysts [15]. However, durability is another key parameter for practical applications during the actual operation of energy conversion and storage devices, and its importance even exceeds the activity. Most of the Ru/RuO_2-based OER catalysts reported at present are mostly stable only for tens or nearly hundreds of hours at low current densities, and the stability maintenance time is drastically shortened when the current density is increased [16,17]. However, with the urgent need for energy transition, the development of OER catalysts with excellent activity and stability under acidic conditions is particularly important for cost reduction and efficiency of energy conversion and storage devices [18,19].

* Corresponding authors.
E-mail addresses: yqsu1989@xjtu.edu.cn (Y. Su), iamyhhan@nwpu.edu.cn (Y. Han).
[1] These authors contributed equally to this work.

https://doi.org/10.1016/j.cclet.2025.111016
1001-8417/© 2026 Published by Elsevier B.V. on behalf of Chinese Chemical Society and Institute of Materia Medica, Chinese Academy of Medical Sciences.

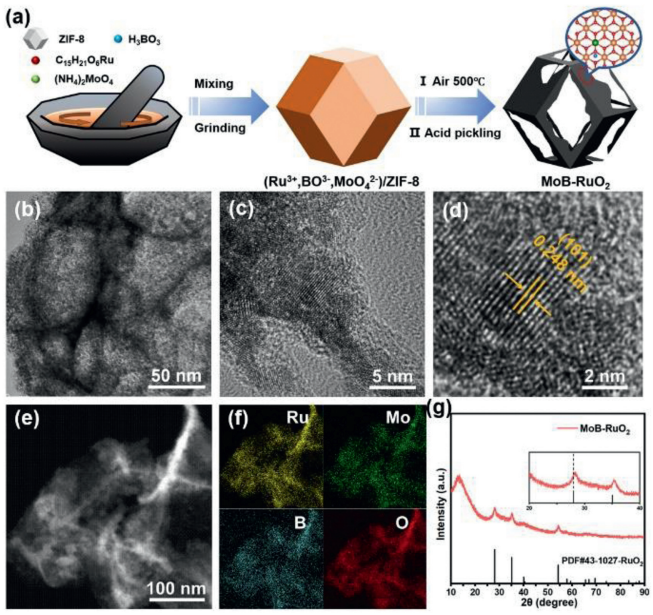


Fig. 1. Preparation and structure characterization of MoB-RuO_2. (a) Schematic diagram of the synthesis MoB-RuO_2. (b-d) HR-TEM images of MoB-RuO_2, and the (101) crystal plane spacing of MoB-RuO_2 marked with the orange line in (d) is 0.248 nm. (e, f) Dark-field HR-TEM image and the corresponding elemental mappings of MoB-RuO_2. (g) XRD pattern of MoB-RuO_2.

Herein, we reported a RuO_2 catalyst co-doped with metallic Mo atoms and non-metallic B atoms (MoB-RuO_2) prepared by a simple mechanical milling method. The catalyst exhibited excellent OER performance in acidic media. The overpotential of MoB-RuO_2 at a current density of 10 mA/cm^2 was only 166 mV, which was much lower than that of commercial RuO_2 catalysts (329 mV). More importantly, MoB-RuO_2 exhibited excellent stability, operating at a current density of 10 mA/cm^2 for at least 550 h with virtually no activity degradation. When used as a PEMWE anode catalyst, PEMWE could operate stably for at least 240 h at a current density of 200 mA/cm^2 (80 °C), exceeding most of the reported catalysts of the same type. Experimental and theoretical calculations showed that the introduction of B atoms resulted in the coordination unsaturation of the Ru active site, greatly optimizing the activity of the catalyst. Additionally, the co-doping of Mo and B atoms optimized the electronic structure of the Ru active site, preventing it from being over-oxidized and dissolved during acidic OER, thus maintaining the stability of the catalyst.

The method for synthesizing MoB-RuO_2 is shown in Fig. 1a, with details of the experiment provided in the Supplementary materials. To begin with, the prepared ZIF-8 is evenly ground with ruthenium acetylacetonate, ammonium molybdate, and boric acid in a mortar. Then the mixture is oxidized and pyrolyzed at low temperature for a long time in the air atmosphere. Finally, zinc oxide is washed off with dilute HCl to obtain Mo and B co-doped RuO_2 catalyst (MoB-RuO_2). Transmission electron microscopy (TEM) images show that MoB-RuO_2 inherited the overall morphology of the ZIF-8 precursor to a large extent, only slightly fragmented (Fig. S1 in Supporting information). As shown in Figs. 1b and c, high-resolution transmission electron microscopy (HR-TEM) images indicate that MoB-RuO_2 is composed of uniform RuO_2 nanoparticles that appear as dodecahedral prisms of ZIF-8. From Fig. 1d, we can observe the lattice spacing of MoB-RuO_2 is 0.248 nm (101), which is reduced compared with that of 0.255 nm for the standard RuO_2, implying that Mo atoms with smaller ion radii are successfully doped into the lattice of RuO_2. The corresponding energy dispersive X-ray (EDX) elemental distributions (Figs. 1e and f) illustrate the homogeneous distribution of Ru, Mo, B, and O elements in the catalysts, further demonstrating the successful co-doping of Mo and B atoms. As shown in Fig. 1g, the X-ray diffraction (XRD) pattern of the prepared MoB-RuO_2 is consistent with the characteristic diffraction peaks of the standard RuO_2 (PDF #43–1025), but the diffraction peaks of MoB-RuO_2 are slightly shifted to a higher angle (Fig. 1g), indicating a contraction of the lattice spacing and further demonstrated the successful introduction of Mo and B atoms [20,21]. The blue shift of characteristic peaks in the Raman spectra of MoB-RuO_2 and RuO_2 also indicate the successful introduction of Mo and B atoms (Fig. S2 in Supporting information) [22]. According to inductively coupled plasma mass spectrometry (ICP-MS, Table S1 in Supporting information), the contents of Ru, Mo, and B were 71.85 %, 4.63 %, and 0.065 %, respectively. Additionally, we used the similar method to synthesize B-RuO_2, Mo-RuO_2, and RuO_2 catalysts as control examples. The morphology characterizations, XRD, and EDX of these samples are shown in Figs. S3-S7 (Supporting information).

The surface chemical states of the samples are characterized by X-ray photoelectron spectroscopy (XPS). Fig. 2a displays the 3p spectra of Ru for MoB-RuO_2 and pure RuO_2 showing two peaks at 484.8 and 463.6 eV, attributed to Ru^{4+} $3p_{1/2}$ and Ru^{4+} $3p_{3/2}$, respectively [23]. The binding energy of MoB-RuO_2 is shifted by 0.4 eV towards a lower binding energy compared to RuO_2, and the same shift can be observed in the Ru 3d spectra (Figs. S8 and S9 in Supporting information), indicating that Ru received electrons and the valence state is lowered, thus helping to prevent over-oxidation of Ru species. According to the Mo 3d spectrum (Fig. 2b), we can observe that Mo exists mainly in the form of Mo^{6+} in MoB-RuO_2 [24]. An oxidized B species can be seen in Fig. S10 (Supporting information), which exists in the form of B-O bond. The presence of high valence Mo and B in MoB-RuO_2 suggested that they provided electrons to the Ru species and prevented them from being over-oxidized during OER process. As shown in Fig. 2c, the O 1s spectrum is convolved into three peaks at 529.4, 530.0, and 531.5 eV for lattice oxygen, Ru-OH, and oxygen vacancy (O_v), respectively [25]. Compared with Mo-RuO_2, the O_v on the MoB-RuO_2 surface increased dramatically after doping with B atoms, which implies an increase in the number of coordination unsaturation of the Ru active centre in MoB-RuO_2 (Fig. S11 in Supporting information), and we speculate that it may be the main reason why MoB-RuO_2 exhibits the most excellent OER catalytic activity. The electron paramagnetic resonance (EPR) further confirms the increase in oxygen vacancies in MoB-RuO_2 (Fig. S12 in Supporting information).

To further investigate the atomic level structural information of MoB-RuO_2, X-ray absorption spectroscopy (XAS) technique was performed. The X-ray absorption near-edge structures (XANES) of MoB-RuO_2 as well as the reference samples Ru foil and RuO_2 were shown in Fig. 2d, where we found that the K-edge absorption of Ru in MoB-RuO_2 is essentially the same as that of RuO_2, and only the absorption edge of Ru in MoB-RuO_2 is slightly lower than that of RuO_2, however, indicating that the valence of Ru in MoB-RuO_2 is slightly lower than that of +4. Fig. 2f compares the XANES spectra of MoB-RuO_2 and reference samples (Mo foil, MoO_2, and MoO_3), we observe that the absorption on the Mo K-edge in MoB-RuO_2 is between MoO_2 and MoO_3, and closer to that of MoO_3. The result is consistent with the results of the XPS analysis. Fig. 2e shows the Fourier transform extended X-Ray absorption fine structure (FT-EXAFS) on the Ru K-edge of MoB-RuO_2, in which the obvious prominent peak at 1.68 Å can be attributed to the Ru-O bond after comparing it with the RuO_2 reference. It is noteworthy that the length of Ru-O bonds in MoB-RuO_2 is longer than that in the RuO_2 reference, which implies that the introduction of Mo and B atoms modulates the electronic structure of the Ru active centre and reduces the covalency of the Ru-O bonds, which contributes to the

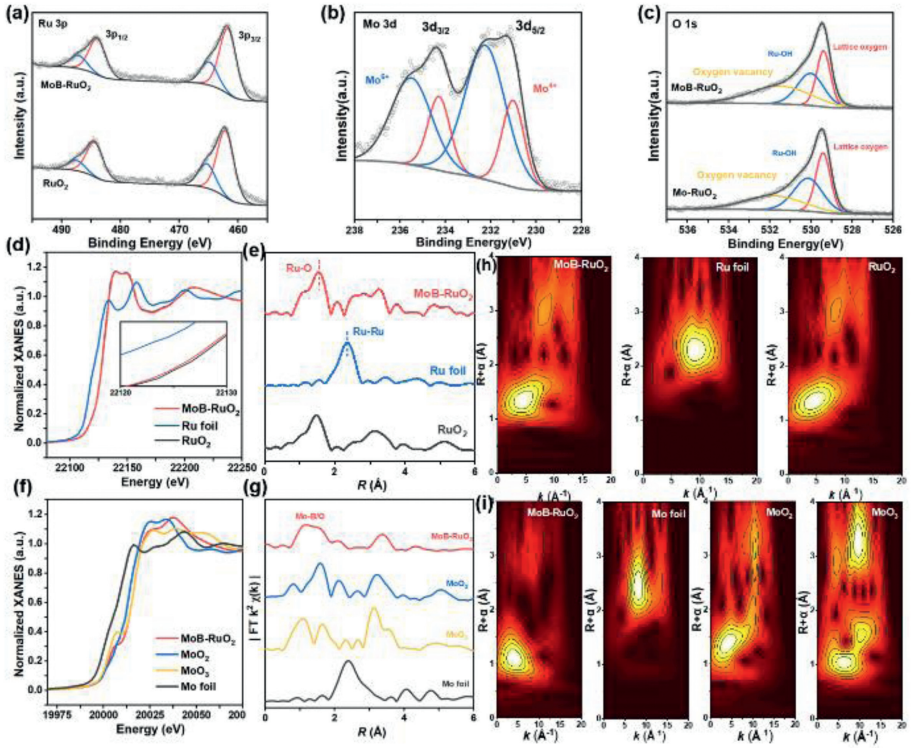


Fig. 2. Structural characterization of MoB-RuO_2. (a) Ru 3p XPS spectra of MoB-RuO_2 and pure RuO_2. (b) Mo 3d XPS spectra of MoB-RuO_2. (c) O 1s XPS spectra of MoB-RuO_2 and Mo-RuO_2. (d) The Ru K-edge XANES spectra of MoB-RuO_2, Ru foil, and RuO_2. (f) The Mo K-edge XANES spectra of MoB-RuO_2, MoO_2, MoO_3, and Mo foil. FT-EXAFS spectra at the (e) Ru K-edge and (g) Mo K-edge of MoB-RuO_2. (h) Ru K-edge wavelet transform-EXAFS of MoB-RuO_2, Ru foil, and RuO_2. (i) Mo K-edge wavelet transform-EXAFS of MoB-RuO_2, MoO_2, MoO_3, and Mo foil.

enhancement of the stability of the catalyst. As shown in Fig. 2g, for FT-EXAFS on the Mo K-edge of MoB-RuO_2, there is a main peak at 1.74 Å, which is like the Mo-O scattering of the first shell in MoO_3. It confirms that the Mo atoms in MoB-RuO_2 is in the oxidation state with +6 valence, which is also consistent with the XPS analysis (Fig. 2b). The Ru K-edge EXAFS spectra were further wavetransformed (WT) to identify the surrounding coordination of the Ru atoms (Fig. 2h). The WT contours of MoB-RuO_2 show a characteristic peak at 4.9 Å^{-1} for the Ru-O bond, which is like that of RuO_2 but different from that of the Ru-Ru bond in Ru foils. In addition, the WT results for Mo are shown in Fig. 2i. Unlike the maximum intensity of Mo foil, the characteristic peak intensity position of Mo at 4.7 Å^{-1} is like that of MoO_3, proving that its oxidation state is +6 valence. The fitting of FT-EXAFS further confirms the previous speculation that the average coordination number of the Ru-O bond is 3.76, slightly smaller than the 4-coordination of the Ru-O bond in standard RuO_2. Additionally, the presence of Ru-O-B/Mo bridge bonds is found in the second-shell of Ru (Fig. S13 and Table S3 in Supporting information). These pieces of evidence indicate that doping with B can alter the coordination imbalance of the active center Ru and obtain more O_v.

The OER performance of MoB-RuO_2 was tested in N_2-saturated 0.5 mol/L H_2SO_4. Fig. 3a shows the linear sweep voltammetry (LSV) curves of MoB-RuO_2 and the control samples. Among them, MoB-RuO_2 shows the best OER performance with an overpotential of 166 mV at 10 mA/cm^2 current density, which is superior to most of the reported catalysts of the same type (Fig. 3b and Table S2 in Supporting information). We believe that the introduction of B atoms leads to the presence of abundant unsaturated coordination Ru sites in MoB-RuO_2, which contributes to the improvement of the OER activity of MoB-RuO_2. Additionally, we find that the kinetic activity of MoB-RuO_2 is significantly increased by the addition of Mo atoms, but the OER activity is not obviously improved. It is evident from Fig. 3c that the Tafel slope of MoB-RuO_2 is 56.2 mV/dec, which is much lower than that of 73.2 mV/dec for B-RuO_2, 67.5 mV/dec for Mo-RuO_2, 75.9 mV/dec for pure RuO_2, and 104.5 mV/dec for commercial RuO_2, suggesting that it has the best kinetic activity. Based on the electrochemical impedance spectra, we find that MoB-RuO_2 has the lowest impedance, which means that the charge transfer resistance is the smallest. Thus, it can be reasonably deduced that the introduction of Mo atoms can effectively improve the impedance of the catalysts and optimize the kinetic activity of MoB-RuO_2 (Fig. S14 in Supporting information).

The stability of the catalyst is very important to evaluate whether it can be used in practical applications. Given that, we first performed accelerated durability test (ADT) to assess the stability of MoB-RuO_2. As shown in Fig. S15 (Supporting information), the LSV curve of MoB-RuO_2 does not shift significantly after 2000 cycles of cyclic voltammetry (CV) test at a scanning speed of 100 mV/s, indicating the excellent OER stability of MoB-RuO_2. In addition, the stability of MoB-RuO_2 is also measured by chronoamperometry to get a more comprehensive understanding of the catalyst stability, and MoB-RuO_2 can be operated stably for at least 550 h at 10 mA/cm^2 current density with almost no degradation of activity (Fig. 3d). However, for B-RuO_2, Mo-RuO_2 and commercial RuO_2, their stability only remains stable for 20, 40 and 40 h, respectively, under similar conditions. Moreover, we also tested the stability at different current densities (at 10, 50, and 100 mA/cm^2 current densities, respectively) (Fig. S16 in Supporting information), it is worth noting that MoB-RuO_2 can work continuously for 300 h at 200 mA/cm^2 without a significant decrease in activity (Fig. 3f). We characterized MoB-RuO_2 after the stability test, and according to the TEM and XPS results, the morphology and elemental valence states of MoB-RuO_2 hardly changed before and after the reaction, which proved that our prepared MoB-RuO_2 has an excellent stability (Figs. S17 and S18 in Supporting information). Most impor-

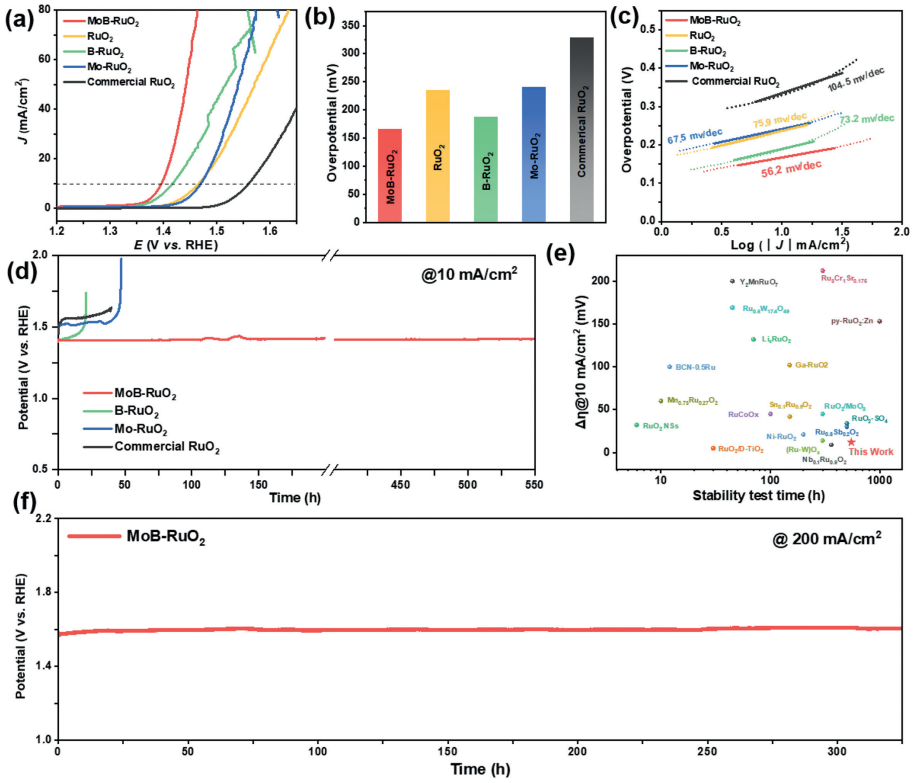


Fig. 3. Electrocatalytic OER performance in acidic media. (a-c) LSV curves, overpotentials at the current density of 10 mA/cm^2, and Tafel plots for MoB-RuO_2, B-RuO_2, Mo-RuO_2, RuO_2, and commercial RuO_2. (d) Chronopotentiometry test at 10 mA/cm^2 current density. (e) Comparison of stability between MoB-RuO_2 and recently reported Ru-based OER electrocatalysts. (f) The chronopotentiometry test of MoB-RuO_2 at the current density of 200 mA/cm^2.

tantly, the OER activity and stability of MoB-RuO_2 also ranked top in comparison with recently reported catalysts of the same type (Fig. 3e, Fig. S19 and Table S2 in Supporting information) [4,13–15,17,23,25–37].

In order to further explain the catalytic mechanism of MoB-RuO_2 under acidic condition, the intermediates during the acidic OER process were investigated using *in situ* attenuated total reflectance Fourier-transform infrared spectroscopy (ATR-FTIR), as shown in Fig. S20 (Supporting information), which displayed the spectra of MoB-RuO_2 during the potential scanning at 1.1−1.9 V. A clear absorption peak of *OOH intermediates at 1051 cm^{-1} was observed when the potential reached only a low voltage of 1.3 V [38]. The intensity of the absorption peaks increased with increasing voltage, and a *OH-related absorption peak (Fig. S21 in Supporting information) was present at 3160–3500 cm^{-1} [39]. This process was consistent with the adsorption evolution mechanism (AEM), which had been widely accepted for acidic OER reactions of RuO_2-based catalysts [40,41]. This was believed to be the reason for its excellent stability in acidic OER.

To verify the catalytic mechanism of MoB-RuO_2 under acidic conditions, we prepare 0.5 mol/L H_2SO_4 using $H_2{}^{18}O$ and $H_2{}^{16}O$ as solvents for two-step *in-situ* differential electrochemical mass spectrometry (DEMS) measurements (see more details in Supporting information). As shown in Fig. S22 (Supporting information), CV cycling testing is conducted in an ^{18}O labeled environment, detecting three products with $m/z = 32$, 34, and 36. Among them, $^{36}O_2$ is the main product, with a small amount of $^{32}O_2$ and $^{34}O_2$ present. After 5 rounds of CV marking, rinse with $H_2{}^{16}O$ to remove unadsorbed $H_2{}^{18}O$. Finally, 5 cycles of LSV testing are conducted in 0.5 mol/L H_2SO_4 using $H_2{}^{16}O$ as the solvent, and the results are shown in Fig. 4a. As the reaction proceeds, the main product is $^{32}O_2$, accompanied by a small amount of $^{36}O_2$ and $^{34}O_2$. According to the calculation of the ratio of $^{36}O_2$ to $^{34}O_2$, the result in Fig. S24 (Supporting information) shows that the value of $^{36}O_2/^{34}O_2$ fluctuates around 0.1 %, which is considered to be the natural abundance of ^{18}O. However, the release of $^{34}O_2$ is due to the binding of an ^{18}O species adsorbed on the surface during the first step of $H_2{}^{18}O$ labeling with ^{16}O in $H_2{}^{16}O$, and the production of $^{36}O_2/^{34}O_2$ in the first cycle is much higher than the natural abundance of ^{18}O. Nevertheless, the yield ratio of MoB-RuO_2 to ^{34}O was significantly lower compared to the control group of RuO_2 (Fig. S23 in Supporting information) indicating that the doping of Mo and B greatly suppressed the occurrence of lattice oxygen oxidation mechanism (LOM). This suggests that the excellent stability of MoB-RuO_2 comes from the catalytic mechanism dominated by AEM. Additionally, the intensity of $^{34}O_2$ decreases as the reaction progresses and the surface ^{18}O is continuously consumed. Therefore, we believe that MoB-RuO_2 follows the AEM mechanism in acidic electrolytes.

Density functional theory (DFT) calculations were conducted to gain a deeper understanding of the catalytic mechanism. To investigate the effect of Mo and B doping on the catalytic activity, Mo and B co-doped RuO_2 (MoB-RuO_2), Mo-doped RuO_2 (Mo-RuO_2), and B-doped RuO_2 (B-RuO_2) models were established based on the standard RuO_2 (101). The optimized structures of the different dopants are shown in Fig. 4c. Due to B entering the RuO_2 lattice and coordinating with O atoms, the original lattice undergoes distortion, and O_v was generated near the Ru site. The Ru site as shown in Fig. S25 (Supporting information) was selected as the active centre, and the reason why the introduction of O_v improved the catalytic activity was theoretically verified.

In-situ DEMS analysis indicated that the acidic OER mechanism was calculated using the AEM pathway, which involved three oxygen-containing intermediates in sequence: *OH, *O, and *OOH. The corresponding adsorption intermediate structure is shown in Figs. S25-S28 (Supporting information). The free-energy diagrams

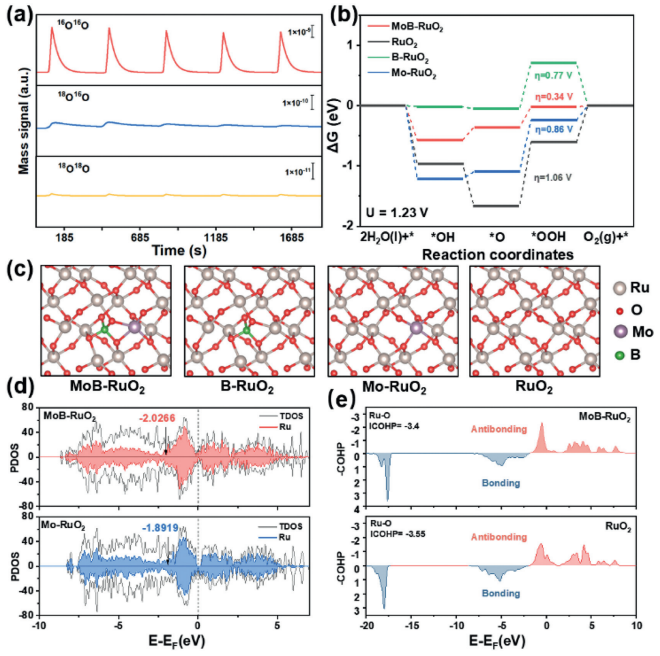


Fig. 4. Mechanism and theoretical analysis. (a) *In-situ* DEMS signals of the generated $^{32}O_2$, $^{34}O_2$, and $^{36}O_2$ *versus* time when performing LSV tests in $H_2{}^{16}O$ electrolyte for ^{18}O-surface labeled MoB-RuO_2. (b) Calculated free-energy diagrams for OER on MoB-RuO_2 surfaces. (c) DFT-optimized structures of MoB-RuO_2, B-RuO_2, Mo-RuO_2 and RuO_2. (d) PDOS of d-bands of active Ru for MoB-RuO_2 and Mo-RuO_2; corresponding d-band centres are denoted by arrows. (e) COHP of active Ru for MoB-RuO_2 and RuO_2.

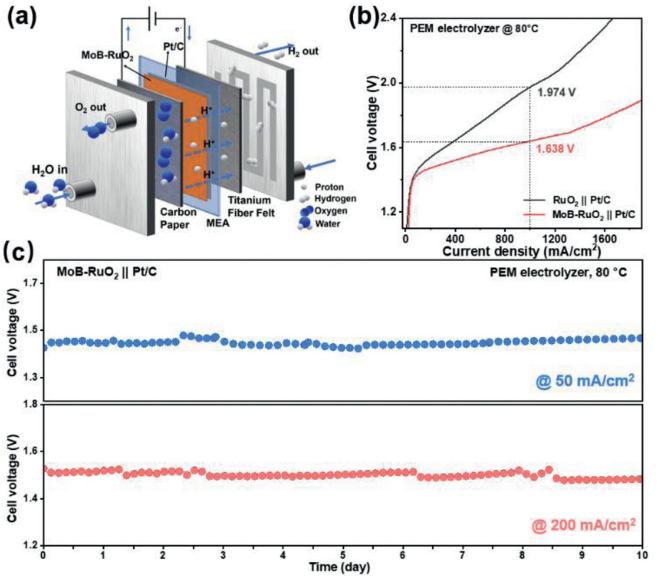


Fig. 5. Performance of PEMWE device. (a) Schematic illustration of the PEM electrolyzer. (b) Polarization curves of the PEM electrolyzers using MoB-RuO_2 or RuO_2 as anode catalyst and commercial Pt/C as a cathodic catalyst at 80 °C. (c) Chronoamperometry of the PEM electrolyzer with MoB-RuO_2 as anode at current density of 50 and 200 mA/cm^2.

of RuO_2 catalysts for OER at $U = 0$ V and $U = 1.23$ V (*vs.* RHE) were calculated (Fig. S29 in Supporting information and Fig. 4b). As shown in Fig. 4b, the formation of *OOH were all rate-determining steps for each catalyst, and the magnitude of the difference in Gibbs free energy (ΔG_{*OOH}-ΔG_{*O}) could reflect the activity of catalysts. The calculated Gibbs free energy barrier of RuO_2 was 1.06 eV, which was considerably higher than that of the other three doped modified RuO_2 materials. The energy barriers of MoB-RuO_2 and B-RuO_2 were lower than those of Mo-RuO_2, which was consistent with the results of electrochemical testing. This suggested that the doping of B could markedly enhance the activity of RuO_2 in acidic OER reactions, moreover, MoB-RuO_2 had a minimum rate-determining step energy barrier of 0.34 eV, indicating a synergistic effect between Mo and B (Fig. S30 in Supporting information).

To further explain the effect of doping on the electronic structure of Ru sites, the projected density of states (PDOS) and crystal orbital Hamilton population (COHP) calculations were conducted. In Fig. 4d, the PDOS values of Ru sites in MoB-RuO_2 and Mo-RuO_2 were calculated, and their positions were labeled. Compared with Mo-RuO_2 (-1.89), the d-band centre of Ru sites in MoB-RuO_2 (-2.03) showed a negative shift, which was due to the O_v introduced by B doping causing the d-band centre to be far away from the Fermi level. The d-band centre of the active site in the OER reaction was far away from the Fermi level, which weakened the chemical bond between it and the adsorbed oxygen-containing intermediate. These all corresponded to a reduction in the free energy barrier, which was beneficial for improving the OER reaction kinetics. This was also confirmed in the calculation of the COHP of Ru-O bonds (Fig. 4e), with the integrated COHP (ICOHP) value of -3.4 for MoB-RuO_2 and -3.55 for RuO_2. This indicated that the bonding ability between surface Ru atoms and O atoms in MoB-RuO_2 was weaker, that is, the adsorption capacity for *O was weaker, resulting in a lower energy barrier for acidic OER reactions. Overall, calculations showed that the excellent OER activity of MoB-RuO_2 mainly came from the introduction of B atoms, which led to the unsaturated coordination of the active center Ru. The doping of Mo and B atoms jointly regulated the electronic structure of the active center Ru, resulting in excellent stability of the catalyst.

To examine the potential of MoB-RuO_2 for practical operation, we assembled PEMWE device with MoB-RuO_2 and commercial Pt/C as anode and cathode, respectively, and evaluated the performance of the device (Fig. 5a). A PEMWE with commercial RuO_2 as anode was also assembled as a control and tested under the same operating conditions. Based on the steady-state polarization curves (Fig. 5b), it is shown that the PEMWE device with MoB-RuO_2 as anode was able to achieve current density of 1000 mA/cm^2 at potential of 1.638 V, which are far superior to that of the PEMWE device with a commercial RuO_2 anode. However, compared to commercial PEMWE devices, the maturity of the preparation of lab-scale devices is far lower mature than that of commercial ones, making the overpotential still slightly insufficient. Excitingly, the MoB-RuO_2 anode-based PEMWE device showed excellent long-term stability (Fig. 5c), which can be operated stably for at least 240 h at 50 and 200 mA/cm^2 current density and operating temperature with almost negligible degradation of the performance. Compared to other Ru based catalysts reported in the past two years, the stability of MoB-RuO_2 in PEMWE is at the front rank (Table S4 in Supporting information). In sum, the doping of Mo and B atoms effectively optimizes the activity and stability of RuO_2, making it a potential candidate for commercialization.

In summary, we synthesized a RuO_2 catalyst doped with Mo and B, which exhibited excellent acidic OER catalytic activity and stability. According to the experimental and DFT calculation results, the introduction of Mo and B can regulate the electrical structure of the Ru catalytic center. By doping with B, oxygen vacancies are introduced into RuO_2, causing the d-band center of nearby Ru sites to move away from the Fermi level, thereby reducing the adsorption of oxygen-containing intermediates by the catalyst and enhancing the catalytic activity of OER reaction. Through the doping of Mo, the electron transfer between Ru and Mo can further reduce the valence state of Ru sites, which can effectively avoid the dissolution of RuO_2 under acidic conditions, thus obtaining extremely excellent stability. PEMWEs assembled with MoB-RuO_2 showing

superb performance and excellent durability in acidic media for water splitting. This finding offers a novel strategy for the rational design and synthesis of high-performance electrocatalysts for the OER in acidic environments.

Declaration of competing interests

The authors declare that they have no known competing financial interests or personal relationships that could have appeared to influence the work reported in this paper.

CRediT authorship contribution statement

Ziang Shang: Writing – original draft, Project administration, Methodology, Investigation, Data curation, Conceptualization. **Heyu Sui:** Writing – original draft, Methodology, Investigation, Data curation. **Zeyi Huang:** Writing – original draft, Methodology, Data curation, Conceptualization. **Xueting Feng:** Methodology, Data curation. **Guanzhen Chen:** Writing – original draft, Methodology. **Jiena Weng:** Validation, Resources, Methodology. **Yu Xiong:** Resources, Methodology. **Yaqiong Su:** Writing – review & editing, Resources, Methodology. **Yunhu Han:** Writing – review & editing, Supervision, Investigation, Funding acquisition, Data curation, Conceptualization.

Acknowledgments

This work is supported by the National Natural Science Foundation of China (No. 22102132), the Funds for Basic Scientific Research in Central Universities, Sponsored by Innovation Foundation for Doctor Dissertation of Northwestern Polytechnical University (No. CX2024101) and Sponsored by the Practice and Innovation Funds for Graduate Students of Northwestern Polytechnical University (No. PF2024029). Y. Su acknowledges the “Young Talent Support Plan” of Xi’an Jiaotong University. Supercomputing facilities were provided by Hefei Advanced Computing Center and Computing Center in Xi’an.

Supplementary materials

Supplementary material associated with this article can be found, in the online version, at doi:10.1016/j.cclet.2025.111016.

References

[1] L. Chong, G. Gao, J. Wen, et al., Science 380 (2023) 609–616.
[2] G. Chen, W. Chen, R. Lu, et al., J. Am. Chem. Soc. 145 (2023) 22069–22078.
[3] X. Feng, G. Chen, Z. Cui, et al., Angew. Chem. Int. Ed. 63 (2024) e202316314.
[4] L. Zhou, Y. Shao, F. Yin, et al., Nat. Commun. 14 (2023) 7644.
[5] M.T.M. Koper, Chem 660 (2011) 254–260.
[6] Y. Wu, Y. Zhao, P. Zhai, et al., Adv. Mate. 34 (2022) 2202523.
[7] S. Liu, H. Tan, Y.C. Huang, et al., Adv. Mater. 35 (2023) 2305659.
[8] Y. Wang, M. Zhang, Z. Kang, et al., Nat. Commun. 14 (2023) 5119.
[9] H. Sun, M. Zhao, C. Ma, et al., Nano Res. 16 (2023) 4980–4986.
[10] Y.Y. Guo, Y.H. Cao, J.D. Lu, et al., Microstructures 3 (2023) 2023038.
[11] X. Xie, L. Du, L. Yan, et al., Adv. Funct. Mater. 32 (2022) 2110036.
[12] R.Y. Fan, Y.S. Zhang, J.Y. Lv, et al., Small 20 (2024) 2304636.
[13] D. Galyamin, J. Torrero, I. Rodríguez, et al., Nat. Commun. 14 (2023) 2010.
[14] Z.L. Zhao, Q. Wang, X. Huang, et al., Energy Environ. Sci. 13 (2020) 5143–5151.
[15] S. Hao, M. Liu, J. Pan, et al., Nat. Commun. 11 (2020) 5368.
[16] X. Zhao, Z. Li, H. Jang, et al., Small 20 (2024) 2311172.
[17] Z. Shi, J. Li, Y. Wang, et al., Nat. Commun. 14 (2023) 843.
[18] Q. Yao, B. Huang, N. Zhang, et al., Angew. Chem. Int. Ed. 58 (2019) 13983–13988.
[19] R. Gong, B. Liu, X. Wang, et al., Small 19 (2023) 2204889.
[20] H.-R. Zhao, C.Z. Yuan, C. Zhou, et al., J. Energy Chem. 94 (2024) 458–465.
[21] X. Ping, Y. Liu, L. Zheng, et al., Nat. Commun. 15 (2024) 2501.
[22] C. Zhao, Y. Huang, B. Jiang, et al., Adv. Energy Mater. 14 (2024) 2302586.
[23] X. Wang, H. Jang, S. Liu, et al., Adv. Energy Mater. 13 (2023) 2301673.
[24] Y. Liu, X. Zhu, Q. Zhang, et al., J. Mater. Chem. A 8 (2020) 8920–8926.
[25] X. Bai, X. Zhang, Y. Sun, et al., Angew. Chem. Int. Ed. 62 (2023) e202308704.
[26] L. Deng, S.F. Hung, S. Liu, et al., J. Am. Chem. Soc. 146 (2024) 23146–23157.
[27] W. Gou, S. Zhang, Y. Wang, et al., Energy Environ. Sci. 17 (2024) 6755–6765.
[28] L. Wu, W. Huang, D. Li, et al., Angew. Chem. Int. Ed. 64 (2025) e202413334.
[29] H. Liu, Z. Zhang, J. Fang, et al., Joule 7 (2023) 558–573.
[30] Y. Qin, B. Cao, X.Y. Zhou, et al., Nano Energy 115 (2023) 108727.
[31] K. Wang, Y. Wang, B. Yang, et al., Energy Environ. Sci. 15 (2022) 2356–2365.
[32] X. Wang, X. Wan, X. Qin, et al., ACS Catal. 12 (2022) 9437–9445.
[33] Y. Duan, L.L. Wang, W.X. Zheng, et al., Angew. Chem. Int. Ed. 63 (2024) e202413653.
[34] Z. Liu, H. Liu, T. Xue, et al., Nano Lett. 24 (2024) 10899–10907.
[35] Z.Y. Wu, F.Y. Chen, B. Li, et al., Nat. Mater. 22 (2023) 100–108.
[36] D. Zhang, M. Li, X. Yong, et al., Nat. Commun. 14 (2023) 2517.
[37] W. Zhu, F. Yao, K. Cheng, et al., J. Am. Chem. Soc. 145 (2023) 17995–18006.
[38] Y. Hao, S.F. Hung, W.J. Zeng, et al., J. Am. Chem. Soc. 145 (2023) 23659–23669.
[39] N. Han, X. Zhang, C. Zhang, et al., Matter 7 (2024) 1330–1343.
[40] Y. Wang, Y. Wen, Y. Cheng, et al., Nano Res. 17 (2024) 1165–1172.
[41] Z.J. Zhang, J.P. Guo, S.H. Sun, et al., Rare Met. 42 (2023) 3607–3613.